# Integral Equation Formulation for Planar Plasmonic Structures With Finite Thickness in Layered Media

Esraa M. Mahdy, Alaa K. Abdelmageed, and Ezzeldin A. Soliman, *Senior Member, IEEE*

***Abstract*—A detailed Volume Integral Equation (VIE) formulation for planar plasmonic nano structures with finite thickness in flat multi-layers medium is presented. The boundary condition along the localized metallic objects is expressed in terms of the unknown polarization current flowing through these objects in the form of an integral equation, which is solved using the Method of Moments (MoM). The Green's functions associated with a layered medium of practical importance are expressed in the spectral domain. The corresponding spatial domain Green's functions are obtained using the Discrete Complex Images Method (DCIM). Special treatment for the spectral function's asymptote at high spectral values is performed. The presented formulation is applied on different plasmonic structures immersed inside layered media. The structures include nano-rod and nano-patch excited by an incident plane wave. In addition, a simple band-stop filter based on quarter-wavelength stubs is considered. This filter is fed with a couple of plasmonic transmission lines. The obtained current distributions and *S*-parameters are compared with those obtained using a commercial full-wave electromagnetic simulator, namely CST Microwave Studio. A very good agreement is observed. The proposed integral equation formulation enjoys high degree of stability, numerical efficiency, and accuracy.**

***Index Terms*—Integral equation formulation, method of moments, green's functions, layered media, plasmonics, nano antennas.**

## I. Introduction

RECENT advances in fabrication technology allows the reduction of the device's dimensions down to the nano-scale At this scale, the high power dissipation is a significant problem for classical electronic devices. Photonic components can be considered as substitute due to their wide operational bandwidth and low power dissipation. However, the diffraction limit of light constrains the dimensions to be in the order of micrometers. Recently, plasmonic devices overcome this problem as they enable the confinement of the light down to the nanoscale, which bridges the size gap between electronic and optical devices. This opened the gate for several plasmonic applications such as sensing and spectroscopy applications [1]–[5], nano-antennas [3], [6]–[11], waveguides [12]–[17], and enhancing the absorption of photovoltaic solar cells [18]–[20]. At optical and near Infra-Red (IR) frequencies, metals behave like plasma. The Drude model [21] simplifies their behavior as a free electron gas moving in a background of positive metallic ions. Consequently, their response can be modeled via a complex frequency-dependent relative permittivity.

In this paper, a detailed volume integral equation formulation to analyze planar plasmonic devices with finite thickness in multilayered media, is developed. This integral equation is solved numerically. Computational electromagnetics is a discipline that seeks a solution for Maxwell's equations associated with irregular structures, which cannot be solved analytically. There are two main branches of computational electromagnetics, one that depends on the differential form of Maxwell's equations, such as Finite Element Method (FEM) [22]–[24] and Finite Difference Time Domain (FDTD) method [25], [26]. The other depends on the integral formulation of Maxwell's equations, such as the Method of Moments (MoM) [27]–[30]. The FEM and FDTD methods, require discretization of the structure as well as the substrate and surrounding media. Thus, the number of unknowns and memory storage as well as the computation time are big. Moreover, these techniques have another disadvantage in solving problems with open boundaries, as a Perfectly Matched Layer (PML) is required to truncate the computational domain, which may result in numerical errors.

On the contrary, the MoM requires discretization of the finite metal structures only. Thus, the number of unknowns and the needed storage are relatively small. The MoM is perfectly suited for structures with open boundaries as no truncation for the computational domain is needed. However, in comparison with the other two methods, the MoM requires more analytical work. Hence, it isn't frequently used if compared with FDTD and FEM in the field of plasmonics. The MoM has been used in the field of plasmonics to solve the Surface Integral Equations (SIEs) associated with various plasmonic structures. SIE relies on the electromagnetic equivalence principle to simplify the treatment of plasmonic volumetric structures. In [31], SIE is formulated for calculating the near and scattered fields of plasmonic structures illuminated with incident plane waves. Another SIE is presented in [32], where multiregion piecewise vector basis functions are used. Such basis functions are convenient for meshing relatively complex composite structures having multiple junctions. The scattered field due to plane wave excitation of different structures is obtained. An enhanced discretization method suitable for sharp-edged plasmonic nano scatterer particles, such as cubes and pyramids, is presented in [33]. Various SIEs applied on

Manuscript received November 23, 2021; revised February 18, 2022; accepted March 6, 2022. Date of publication March 10, 2022; date of current version March 31, 2022. *(Corresponding author: Ezzeldin A. Soliman.)*

Esraa M. Mahdy and Alaa K. Abdelmageed are with the Department of Engineering Mathematics and Physics, Faculty of Engineering, Cairo University, Giza 12211, Egypt (e-mail: emahdy@cu.edu.eg; abdelmag@msn.com).

Ezzeldin A. Soliman is with the Department of Physics, School of Sciences and Engineering, The American University in Cairo, New Cairo 11835, Egypt (e-mail: esoliman@aucegypt.edu).

Digital Object Identifier 10.1109/JPHOT.2022.3158399

This work is licensed under a Creative Commons Attribution 4.0 License. For more information, see https://creativecommons.org/licenses/by/4.0/

various plasmonic nano scatterers are compared in [34], [35]. The different iterative solvers used to solve the corresponding system of linear equations are compared in [35]. The MoM is also used to solve the SIE of plasmonic transmission lines in free-space [36] and layered media [37]. Plasmonic transmission lines are open structures in one direction, that is the longitudinal direction of the wave propagation, while finite in the other two transversal directions. The associated Green's functions are due to wire, filament, sources instead of the conventional point sources used for analyzing finite structures in all directions.

If higher accuracy and more flexibility in the shape of the plasmonic structure under investigation are needed, SIE has to be replaced with Volume Integral Equation (VIE) to be solved also using the MoM. VIE formulation requires more analytical work, computer memory, and simulation time if compared to SIE. Consequently, VIE has less share in plasmonics' literature relative to SIE formulation. The electric volume current inside a plasmonic scatterer is solved for via VIE in [38]. Surface plasmon resonance due to plane wave illumination of cylinders and stars with different cross-sectional geometries embedded inside homogeneous medium are analyzed. The propagation of surface plasmon polaritons in planar layered media due to excitation with near line sources is studied using VIE in [39]. Another VIE is formulated in [40] to solve for the dispersion characteristics of plasmonic photonic crystals in layered media. Thin-film solar cells with embedded plasmonic nano particles is analyzed in [41] making use of a VIE formulation. The absorption enhancement within the active region of solar cell due to illumination with sunlight is obtained.

The VIE formulation proposed is this paper has several appealing features such as: 1) Closed-forms of the spectral Green's functions of layered medium of practical importance are presented. 2) The corresponding spatial Green's functions for the same frequently used layered medium are analytically expressed. 3) The matrix representation of the formulated VIE is presented, with detailed expressions of the impedance matrix elements. 4) The elements of the excitation vector are fully expressed not only for the conventional plane wave excitation of plasmonic structures, but also for excitation with plasmonic transmission lines terminated with localized current sources, which makes the proposed formulation very suitable for analyzing plasmonic devices such as filters, couplers, splitters, and antennas.

The remainder of the paper is organized as follows. In Section II, the spectral domain Green's functions are defined and expressed. Then, the Discrete Complex Images Method (DCIM) is used to convert the spectral Green's functions back to the spatial domain. In Section III, the integral equation formulation of the category of structures under investigation is presented. The formulated integral equation is then solved using the MoM. The presented technique is applied in Section IV to analyze number of plasmonic planar structures, such as nano-rod and nano-patch antenna in layered medium excited by plane wave. A band-stop filter on top of a grounded substrate and fed with plasmonic transmission lines is also investigated. The results of the presented formulation are always compared with the results obtained by CST Microwave Studio [42]. Finally, the paper is concluded in Section V.

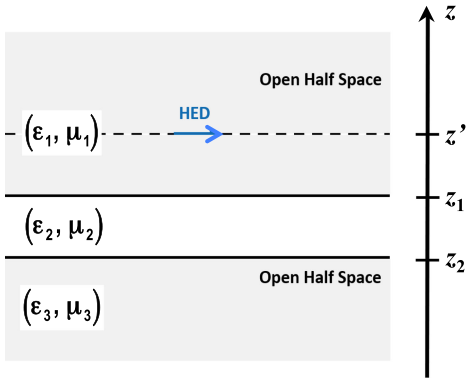


Fig. 1. HED on top of a layered medium.

## II. Green's Functions of Layered Medium

### A. Spectral Domain Green's Functions

Green's functions can be looked at as the impulse response of a system, so they are defined as the electromagnetic fields due to infinitesimal unit current sources. Any general source can be seen as combination of a number of infinitesimal unit sources with different weights. Therefore, the response of a linear system due to a source can be found as the superposition of the responses due to these unit sources. Consequently, the Green's functions are considered as a corner stone for solving electromagnetic problems via integral equation formulation, as demonstrated in Section III. There are closed forms for the Green's functions of a source in free-space [22], while there is no such a straightforward analytical solution for the Green's function for layered media. The first step to obtain the Green's function for a Horizontal Electric Dipole (HED) impressed in a multilayered medium, as shown in Fig. 1, is to solve Maxwell's equations satisfying the boundary conditions at each interface between the layers. Via mapping the problem from the spatial to the spectral domain, Maxwell's equations which are coupled Partial Differential Equations (PDE), are converted into uncoupled second-order Ordinary Differential Equations (ODE) that can be easily solved by analogy to a transmission line problem.

By transforming Maxwell's equations to the spectral domain and calculating the spectral electric field components due the HED shown in Fig. 1, the spectral dyadic Green's functions can be expressed as follows [36]:

$$\tilde{G}_{xx} = \tilde{G}_1 - (jk_x)(jk_x)\tilde{G}_2 \tag{1}$$

$$\tilde{G}_{yy} = \tilde{G}_1 - (jk_y)(jk_y)\tilde{G}_2 \tag{2}$$

$$\tilde{G}_{xy} = \tilde{G}_{yx} = -(jk_x)(jk_y)\tilde{G}_2 \tag{3}$$

where $k_x$ and $k_y$ are the spectral correspondent of the spatial variables $x$ and $y$, respectively, which are the coordinate axes perpendicular to the direction of stratification, $z$-axis. The *basic* spectral Green's functions $\tilde{G}_1$ and $\tilde{G}_2$, where both the source and observation points are located in medium 1, can be expressed as

follows:

$$\tilde{G}_1 = -\frac{\omega\mu_1}{2k_{z1}}\left[e^{\mp jk_{z1}(z-z')} + \Gamma_1^{\mathrm{TE}}\, e^{-jk_{z1}(z+z')}\right] \tag{4}$$

$$\tilde{G}_2 = \frac{1}{2k_{z1}\omega\epsilon_1} \times \left[e^{\mp jk_{z1}(z-z')} + \frac{1}{k_\rho^2}\left(\omega^2\mu_1\epsilon_1\Gamma_1^{TE} + k_{z1}^2\Gamma_1^{TM}\right)\, e^{-jk_{z1}(z+z')}\right] \tag{5}$$

where the –ve and +ve sign in the exponent of the first exponential function in both (4) and (5) correspond to the observation point ($z$) above and below the HED source ($z$'), respectively. $k_{zi}$ is the propagation constant along $z$-direction in the $i$th layer and defined as $k_{zi}^2 = \omega^2\,\mu_i\epsilon_i - k_\rho^2$. $k_\rho$ is the spectral correspondent of the spatial variable $\rho = \sqrt{x^2+y^2}$ , where $k_\rho^2 = k_x^2 + k_y^2$. $\Gamma_i^{\mathrm{TE/TM}}$ is the reflection coefficient in $i$th layer for the TE/TM subsystem taking into account the presence of the entire layered medium, such that:

$$\Gamma_1^{\mathrm{TE/TM}} = \frac{\Gamma_{2,1}^{\mathrm{TE/TM}} + \Gamma_2^{\mathrm{TE/TM}} e^{-j2k_{z2}z_1}}{1 + \Gamma_{2,1}^{\mathrm{TE/TM}}\Gamma_2^{\mathrm{TE/TM}} e^{-j2k_{z2}z_1}}\; e^{j2k_{z1}z_1} \tag{6}$$

$$\Gamma_2^{\mathrm{TE/TM}} = \Gamma_{3,2}^{\mathrm{TE/TM}}\; e^{j2k_{z2}z_2} \tag{7}$$

$$\Gamma_{i,j}^{\mathrm{TE}} = \frac{\mu_i k_{zj} - \mu_j k_{zi}}{\mu_i k_{zj} + \mu_j k_{zi}}\,,\; \Gamma_{i,j}^{\mathrm{TM}} = \frac{\epsilon_i k_{zj} - \epsilon_j k_{zi}}{\epsilon_i k_{zj} + \epsilon_j k_{zi}} \tag{8}$$

### *B. Spatial Domain Green's Functions*

The conversion back to the spatial domain can be done by applying the inverse Fourier transformation on the spectral domain Green's functions, (1)–(3), which leads to the following:

$$G_{xx} = G_1 - \frac{\partial^2}{\partial x^2}G_2 \tag{9}$$

$$G_{yy} = G_1 - \frac{\partial^2}{\partial y^2}G_2 \tag{10}$$

$$G_{xy} = G_{yx} = -\frac{\partial}{\partial x}\frac{\partial}{\partial y}G_2 \tag{11}$$

where $G_1$ and $G_2$ are the spatial counterparts of the spectral functions $\tilde{G}_1$ and $\tilde{G}_2$, respectively. The multiplication by $jk_x$ and $jk_y$ in the spectral domain is converted into $\partial/\partial x$ and $\partial/\partial y$ in the spatial domain, respectively. Applying inverse transformation from the spectral domain back to the spatial domain on (4) and (5), the spatial basic Green's functions can be obtained:

$$G_1 = -\frac{j\omega\mu_1}{4\pi}\int_{-\infty}^{\infty}\left[e^{\mp jk_{z1}(z-z')} + R_1 e^{-jk_{z1}(z+z')}\right] H_0^2\left(k_\rho\rho\right)\frac{k_\rho}{j2k_{z1}}dk_\rho \tag{12}$$

$$G_2 = \frac{j}{4\pi\omega\epsilon_1}\int_{-\infty}^{\infty}\left[e^{\mp jk_{z1}(z-z')} + R_2 e^{-jk_{z1}(z+z')}\right] H_0^2\left(k_\rho\rho\right)\frac{k_\rho}{j2k_{z1}}dk_\rho \tag{13}$$

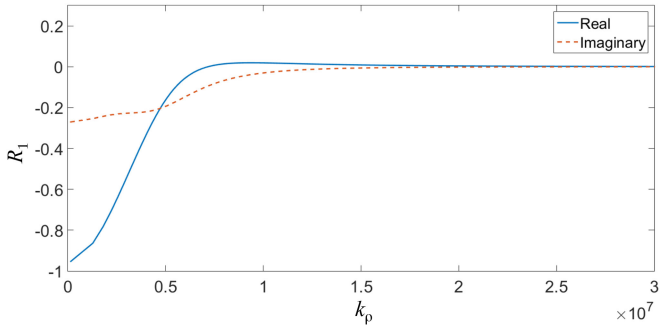


Fig. 2. The spectral function $R_1$ versus the spectral variable $k_\rho$.

where the spectral functions $R_1$ and $R_2$, which are free from $z$ and $z$' dependency, can be expressed as follows:

$$R_1 = \Gamma_1^{\mathrm{TE}} \tag{14}$$

$$R_2 = \frac{1}{k_\rho^2}\left(\omega^2\mu_1\epsilon_1\Gamma_1^{\mathrm{TE}} + k_{z1}^2\Gamma_1^{\mathrm{TM}}\right) \tag{15}$$

The integrals in (12) and (13) are known as Sommerfeld integrals, which are computationally expensive and time-consuming due to the highly oscillatory and slowly decaying integrands. Therefore, the Discrete Complex Images Method (DCIM) [43] is employed in order to avoid evaluating these integrals numerically. In this technique, a spectral domain Green's function is expanded into a summation of number of exponential functions with complex coefficients via the Generalized Pencil-Of-Function (GPOF) [44] method, or Prony's method [45]. The conversion into spatial domain is then accomplished using Sommerfeld identities [46] to obtain the closed form of the spatial Green's function as another summation of exponential contributions from the source's images located at complex distances.

It is worth mentioning that the DCIM is better applied on the spectral functions after extracting the quasi-dynamic terms [47]. This extraction can be done by applying the low frequency limit, where $k_z$ of all media are almost equal. The real and imaginary parts of $R_1$ versus $k_\rho$ are plotted in Fig. 2. As shown in this figure, the quasi-dynamic subtraction is not required for this spectral function $R_1$ as it is rapidly decaying.

On the other hand, Fig. 3(a) and 3(b) show the real and imaginary parts of the second spectral function $R_2$ before and after the subtraction of the quasi-dynamic terms, $R_{2q}$, respectively. Unlike the original function $R_2$, the function $(R_2 - R_{2q})$ is rapidly decaying as desired. The spectral functions presented in Figs. 2 and 3 correspond to a HED located in free-space above a frequently used $SiO_2$/Au substrate. The $SiO_2$ layer has thickness of 500 nm and relative permittivity equals 2.1. The lower-most Au layer is assumed thick enough to act effectively as a half-space with no reflection. The subtracted quasi-dynamic terms, $R_{2q}$, are:

$$R_{2q} = -K_1\, e^{j2k_{z1}z_1} + K_2\left(K_1^2 - 1\right)e^{j2k_{z1}z_2} + K_1K_2^2 e^{-jk_{z1}(2z_1 - 4z_2)} \tag{16}$$

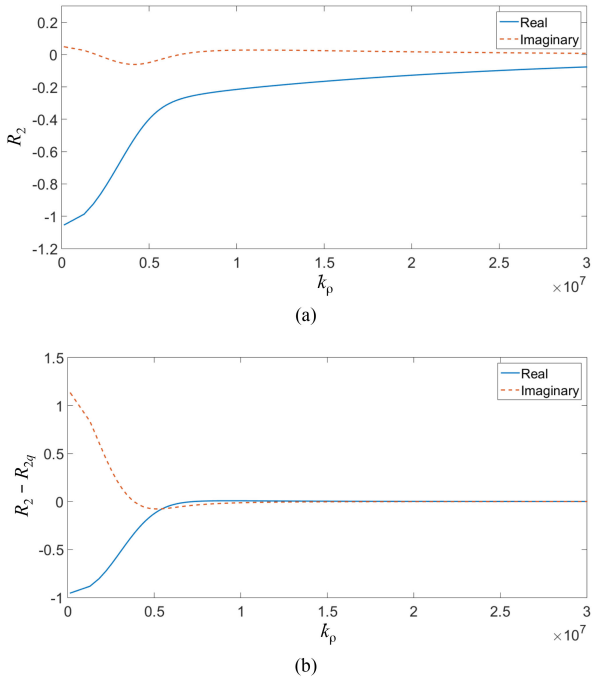


Fig. 3. The spectral function $R_2$ versus the spectral variable $k_\rho$: (a) Before extracting the quasi-dynamic terms. (b) After extracting the quasi-dynamic terms, $R_{2q}$.

where

$$K_1 = \frac{\epsilon_2 - \epsilon_1}{\epsilon_2 + \epsilon_1}\ ,\ K_2 = \frac{\epsilon_3 - \epsilon_2}{\epsilon_3 + \epsilon_2} \tag{17}$$

Applying the aforementioned steps of the DCIM, the integrations appearing in (12) and (13) can be expressed as follows [43]:

$$G_1 = \frac{-j\omega\mu_1}{4\pi}\left(\frac{e^{-jk_1r_1}}{r_1} + \sum_{i=1}^{N_1} a_i \frac{e^{-jk_1r_{i1}}}{r_{i1}}\right) \tag{18}$$

$$G_2 = \frac{j}{4\pi\omega\epsilon_1}\left[\frac{e^{-jk_1r_1}}{r_1} - K_1\frac{e^{-jk_1r_2}}{r_2} + K_2\left(K_1^2 - 1\right)\frac{e^{-jk_1r_3}}{r_3} + K_1K_2^2\frac{e^{-jk_1r_4}}{r_4} + \sum_{i=1}^{N_2} c_i\frac{e^{-jk_1r_{i2}}}{r_{i2}}\right] \tag{19}$$

where

$$r_1 = \sqrt{(x-x')^2 + (y-y')^2 + (z-z')^2} \tag{20}$$

$$r_2 = \sqrt{(x-x')^2 + (y-y')^2 + (z+z'-2z_1)^2} \tag{21}$$

$$r_3 = \sqrt{(x-x')^2 + (y-y')^2 + (z+z'-2z_2)^2} \tag{22}$$

$$r_4 = \sqrt{(x-x')^2 + (y-y')^2 + (z+z'+2z_1-4z_2)^2} \tag{23}$$

$$r_{i1} = \sqrt{(x-x')^2 + (y-y')^2 + (z+z'+jb_i)^2} \tag{24}$$

TABLE I
COEFFICIENTS AND LOCATIONS OF THE COMPLEX IMAGES OF THE SPECTRAL FUNCTION $R_1$

| $i$ | $a_i$ | $b_i \times 10^{-7}$ |
|---|---|---|
| 1 | $-4.8915 - j2.2836$ | $-9.6838 - j9.4793$ |
| 2 | $-0.0335 + j0.0070$ | $3.9521 - j11.666$ |
| 3 | $0.1115 - j0.0818$ | $-0.3684 - j2.0184$ |
| 4 | $1.3254 - j1.8174$ | $-1.8395 - j5.7751$ |

TABLE II
COEFFICIENTS AND LOCATIONS OF THE COMPLEX IMAGES OF THE SPECTRAL FUNCTION $(R_2 - R_{2q})$

| $i$ | $c_i$ | $d_i \times 10^{-7}$ |
|---|---|---|
| 1 | $-1.2587 - j0.8630$ | $-3.1724 - j21.024$ |
| 2 | $0.0750 - j0.0582$ | $-0.4700 - j2.3508$ |
| 3 | $2.5938 - j2.0827$ | $-2.4388 - j7.9615$ |
| 4 | $-3.4907 - j4.5673$ | $-10.911 - j8.8936$ |

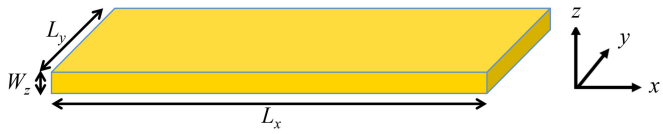


Fig. 4. Gold rod in free-space.

$$r_{i2} = \sqrt{(x-x')^2 + (y-y')^2 + (z+z'+jd_i)^2} \tag{25}$$

The coordinates of the observation and source points are ($x$, $y$, $z$) and ($x'$, $y'$, $z'$), respectively. ($a_i$, $c_i$) and ($b_i$, $d_i$) are the coefficients and locations of the complex images for the spectral functions $R_1$ and $(R_2 - R_{2q})$, respectively, whose values for a source on top of the same $SiO_2$/Au substrate under investigation are listed in Tables I and II, respectively. It is worth mentioning that the $\mp$ sign in (12) and (13) disappears due to squaring the difference between $z$ and $z'$ in (20). This makes the spatial Green's function expressions for observation points above and below the source identical.

The derived form of the basic spatial domain Green's functions in a layered medium, equations (18) and (19), resembles the form of the Green's function due to a source located in free-space. Consequently, when these Green's functions are plugged into the integral equation derived in the following section, the problem of a plasmonic structure in a layered medium, can be looked as a superposition of a number of free-space associated problems.

## III. Integral Equation Formulation and the Method of Moments

The volume integral equation to be satisfied at any point within the volume of a localized plasmonic structure, for example a gold rod with finite thickness in free-space as shown in Fig. 4, is given by [46]:

$$\iiint_{\substack{localized\\metal}} \underline{\underline{G}}^{E,J}(\underline{r},\underline{r}')\ \underline{J}(\underline{r}')\ d\tau' = \frac{\underline{J}(\underline{r})}{j\omega(\hat{\epsilon} - \epsilon_0)} - \underline{E}^i(\underline{r}) \tag{26}$$

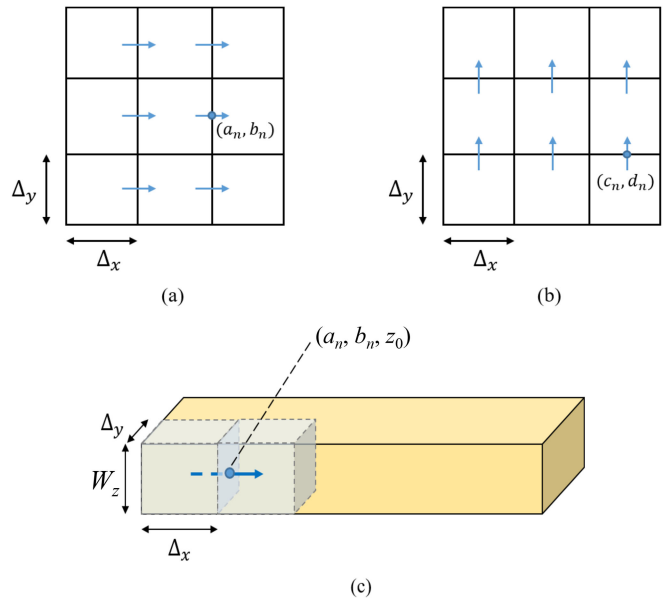


Fig. 5. Rectangular meshing and the basis functions: (a) Basis functions along $x$-direction. (b) Basis functions along $y$-direction. (c) 3D view of an $x$-directed basis function.

where $\underline{r}$ and $\underline{r'}$ are the observation and source points, respectively. $\underline{J}$ represents the unknown induced polarization electric current flowing through the plasmonic metallic structure. $\underline{\underline{G}}^{E,J}$ is the Green's function matrix that links the electric current $\underline{J}$ to the electric field $\underline{E}$ according to (9)–(11). $\epsilon_0$ and $\hat{\epsilon}$ are the permittivity of the free-space and the metal forming the localized plasmonic structure, respectively. The latter permittivity is complex and frequency dependent. It can be calculated using the Drude model [21]. In this study, the experimental results [48] are used as a better alternative. $\underline{E}^i$ represents the excitation electric field, which could be due to an incident plane wave or a localized current source usually located at the far edge of a feeding transmission line.

The MoM starts by the meshing step, where the structure under investigation is subdivided into small segments, as shown in Fig. 5. In this study, rectangular mesh is used with dimensions $\Delta_x$, $\Delta_y$ and $W_z$ along the $x$-, $y$- and $z$-axis, respectively. It is worth mentioning that the structures under investigation in this paper are planar structures with relatively small non-zero thickness, $W_z$, along $z$-direction. Hence, a single mesh cell is assumed along $z$-axis, whose thickness, $W_z$, is the same as that of the entire planar structure. Consequently, there is no need to consider current flowing along $z$-axis.

The second step in the MoM technique is to expand the unknown polarization currents in terms of known basis functions, triangular basis functions (roof-tops), weighted by unknown expansion coefficients. Finally, using testing technique, such as point-matching or Galerkin, (26) is applied at many test points along the metallic structure. By applying these steps, the integral (26) is converted into the following matrix equation, which can be solved using conventional matrix techniques:

$$\begin{bmatrix} [Z_{xx}]_{N_x\times N_x} & [Z_{xy}]_{N_x\times N_y} \\ [Z_{yx}]_{N_y\times N_x} & [Z_{yy}]_{N_y\times N_y} \end{bmatrix} \begin{bmatrix} [C_x]_{N_x\times 1} \\ [C_y]_{N_y\times 1} \end{bmatrix} = \frac{1}{j\omega\left(\hat{\epsilon}-\epsilon_0\right)} \frac{1}{\Delta_x\Delta_y W_z} \begin{bmatrix} [I]_{N_x\times N_x} & [0]_{N_x\times N_y} \\ [0]_{N_y\times N_x} & [I]_{N_y\times N_y} \end{bmatrix} \times \begin{bmatrix} [C_x]_{N_x\times 1} \\ [C_y]_{N_y\times 1} \end{bmatrix} - \begin{bmatrix} [E_x^i]_{N_x\times 1} \\ [E_y^i]_{N_y\times 1} \end{bmatrix} \tag{27}$$

where $[C_x]$ and $[C_y]$ are the unknown current expansion coefficients of the $x$- and $y$-directed basis functions, respectively. $[I]$ and [0] are the identity and zero matrices, respectively. $[E_x^i]$ and $[E_y^i]$ represent the $x$- and $y$-components, respectively, of the excitation electric field. $N_x$ and $N_y$ are the number of basis functions along $x$- and $y$-directions, respectively. $[Z_{xx}]$, $[Z_{xy}]$, $[Z_{yx}]$, and $[Z_{yy}]$ are the sub-matrices of the impedance matrix. Adopting point-matching testing, the elements of these sub-matrices can be expressed as follows:

$$\begin{aligned} Z_{xx}\ (m,n) = & \int_{z_0-\frac{W_z}{2}}^{z_0+\frac{W_z}{2}} dz' \int_{b_n-\frac{\Delta_y}{2}}^{b_n+\frac{\Delta_y}{2}} dy' \int_{a_n-\Delta_x}^{a_n+\Delta_x} dx'\, G_1\big|_{\substack{x=a_m\\y=b_m\\z=z_0}} \\ & \times T\left(x'-a_n\right) R\left(y'-b_n\right) R\left(z'-z_0\right) \\ & - \int_{z_0-\frac{W_z}{2}}^{z_0+\frac{W_z}{2}} dz' \int_{b_n-\frac{\Delta_y}{2}}^{b_n+\frac{\Delta_y}{2}} dy' \int_{a_n-\Delta_x}^{a_n+\Delta_x} dx' \frac{\partial G_2}{\partial x}\bigg|_{\substack{x=a_m\\y=b_m\\z=z_0}} \\ & \times \frac{dT\left(x'-a_n\right)}{dx'} R\left(y'-b_n\right) R\left(z'-z_0\right) \end{aligned} \tag{28}$$

$$\begin{aligned} Z_{xy}\left(m,n\right) = & \\ & - \int_{z_0-\frac{W_z}{2}}^{z_0+\frac{W_z}{2}} dz' \int_{d_n-\Delta_y}^{d_n+\Delta_y} dy' \int_{c_n-\frac{\Delta_x}{2}}^{c_n+\frac{\Delta_x}{2}} dx' \frac{\partial G_2}{\partial x}\bigg|_{\substack{x=a_m\\y=b_m\\z=z_0}} \\ & \times R\left(x'-c_n\right) \frac{dT\left(y'-d_n\right)}{dy'} R\left(z'-z_0\right) \end{aligned} \tag{29}$$

$$\begin{aligned} Z_{yx}\ (m,n) = & \\ & - \int_{z_0-\frac{W_z}{2}}^{z_0+\frac{W_z}{2}} dz' \int_{b_n-\frac{\Delta_y}{2}}^{b_n+\frac{\Delta_y}{2}} dy' \int_{a_n-\Delta_x}^{a_n+\Delta_x} dx' \frac{\partial G_2}{\partial y}\bigg|_{\substack{x=c_m\\y=d_m\\z=z_0}} \\ & \times \frac{dT\left(x'-a_n\right)}{dx'} R\left(y'-b_n\right) R\left(z'-z_0\right) \end{aligned} \tag{30}$$

$$Z_{yy}\left(m,n\right) = \int_{z_0-\frac{W_z}{2}}^{z_0+\frac{W_z}{2}} dz' \int_{d_n-\Delta_y}^{d_n+\Delta_y} dy' \int_{c_n-\frac{\Delta_x}{2}}^{c_n+\frac{\Delta_x}{2}} dx'\, G_1\big|_{\substack{x=c_m\\y=d_m\\z=z_0}}$$

$$\times R(x'-c_n)\,T(y'-d_n)\,R(z'-z_0)$$
$$-\int_{z_0-\frac{W_z}{2}}^{z_0+\frac{W_z}{2}} dz' \int_{d_n-\Delta_y}^{d_n+\Delta_y} dy' \int_{c_n-\frac{\Delta_x}{2}}^{c_n+\frac{\Delta_x}{2}} dx' \left.\frac{\partial G_2}{\partial y}\right|_{\substack{x=c_m\\y=d_m\\z=z_0}}$$
$$\times R(x'-c_n)\,\frac{dT(y'-d_n)}{dy'}R(z'-z_0) \tag{31}$$

where $T$ and $R$ are triangle and rectangular functions, respectively, that are used to expand the unknown current components [36]. $m$ and $n$ are the orders of the test point and the current expansion function, respectively. $(a_n, b_n, z_0)$ and $(c_n, d_n,\ z_0)$ are the coordinates of the centers of the $n$th $x$- and $y$-directed basis functions, respectively, as shown in Fig. 5. $z_0$ is the halfway $z$-coordinate of the metallic structure. The basic Green's functions $G_1$ and $G_2$ for the layered medium under consideration are expressed in (18) and (19), respectively. Substituting these Green's functions into (9)–(11) then into (28)–(31), it is clear that any element in the impedance matrix can be looked at as a superposition of terms similar to the corresponding free-space case.

The elements of the excitation electric field vectors $[E_x^i]$ and $[E_y^i]$ are calculated according to the method of excitation. For a plane wave excitation propagating along –$z$ direction with its electric field polarized along $x$-axis, the excitation field vectors can be written as follows:

$$[E_x^i]_{N_x\times 1} = \begin{bmatrix} E_0 \\ \vdots \\ \vdots \\ E_0 \end{bmatrix}, \quad [E_y^i]_{N_y\times 1} = \begin{bmatrix} 0 \\ \vdots \\ \vdots \\ 0 \end{bmatrix} \tag{32}$$

where $E_0$ is the incident electric filed at the halfway $z$-coordinate of the metallic structure, $z_0$. If the plasmonic structure is to be fed with a transmission line, the excitation is not due to an incident plane wave but due to a localized current source located at the outer edge of the feeding transmission line. This localized current source can be represented by a half-roof-top basis function [49]. Consequently, the elements of the excitation field vectors can be expressed as follows:

$$E_x^i(m) = \int_{z_0-\frac{W_z}{2}}^{z_0+\frac{W_z}{2}} dz' \int_{y_s-\frac{\Delta_y}{2}}^{y_s+\frac{\Delta_y}{2}} dy' \int_{x_s}^{x_s+\Delta_x} dx'\, G_1\big|_{\substack{x=a_m\\y=b_m\\z=z_0}}$$
$$\times T_H(x'-x_s)\,R(y'-y_s)\,R(z'-z_0)$$
$$-\int_{z_0-\frac{W_z}{2}}^{z_0+\frac{W_z}{2}} dz' \int_{y_s-\frac{\Delta_y}{2}}^{y_s+\frac{\Delta_y}{2}} dy' \int_{x_s}^{x_s+\Delta_x} dx' \left.\frac{\partial G_2}{\partial x}\right|_{\substack{x=a_m\\y=b_m\\z=z_0}}$$
$$\times\frac{dT_H(x'-x_s)}{dx'}R(y'-y_s)\,R(z'-z_0) \tag{33}$$

$$E_y^i(m) = -\int_{z_0-\frac{W_z}{2}}^{z_0+\frac{W_z}{2}} dz' \int_{y_s-\frac{\Delta_y}{2}}^{y_s+\frac{\Delta_y}{2}} dy' \int_{x_s}^{x_s+\Delta_x} dx' \left.\frac{\partial G_2}{\partial y}\right|_{\substack{x=c_m\\y=d_m\\z=z_0}}$$
$$\times\frac{dT_H(x'-x_s)}{dx'}R(y'-y_s)\,R(z'-z_0) \tag{34}$$

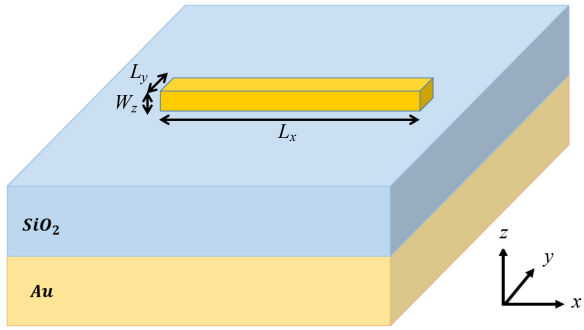


Fig. 6. Gold rod above a finite substrate backed by sufficiently thick gold ground layer.

where $T_H$ is a half-triangular function located at the outer edge of a feeding transmission line oriented parallel to the $x$-axis [49]. The $x$- and $y$-coordinates of this edge are $x_s$ and $y_s$, respectively. If the feeding transmission line is oriented parallel to the $y$-axis, the dual version of (33) and (34) have to be used. After calculating the elements of the impedance matrix and the elements of the excitation electric field vectors, the unknown expansion coefficients of the current $[C]$, can be found by solving (27) using conventional matrix techniques.

## IV. Results and Discussion

### A. Plasmonic Nano Rod Above Finite Substrate Illuminated by Plane Wave

A plasmonic rod, shown in Fig. 6, embedded within a practical supporting layered medium is investigated. The Green's functions for a source in a three-layers medium, specifically air/$SiO_2$/Au, are calculated as presented in Section II. The gold nano rod is located above the $SiO_2$ substrate with relative permittivity of 2.1, thickness of 500 nm, and backed by a sufficiently thick Au ground plane. The rod is excited by a plane wave propagating along the $z$-axis with its incident electric field polarized along the length of the rod, i.e., along $x$-axis, with $E_0$ of 1 V/m. The length $L_x$, width $L_y$, and thickness $W_z$ of the rod are 387.5, 15.5, and 15.5 nm, respectively. These dimensions are equivalent to 0.25 $\lambda_0$ , 0.01 $\lambda_0$ , and 0.01 $\lambda_0$ , respectively, at a frequency of 193 THz whose free-space wavelength $\lambda_0$ is 1550 nm.

The normalized $x$-component of the induced current along the rod axis is calculated at 193 THz and plotted in Fig. 7 together with the results obtained using CST. As can be observed, the comparison between the proposed solver and CST shows a very good matching. The number of mesh cells used by the developed solver to simulate this structure is 65 segments along the longitudinal direction and one segment along the other two perpendicular directions. Significantly large number of segments is taken along the longitudinal direction in order to obtain a smooth current distribution curve. On the other hand, the total number of mesh cells required by CST to simulate the same structure is 516,675. Consequently, the required memory by the proposed solver and CST are 24.8 MB and 183 MB, respectively. The current distribution along the rod shows the

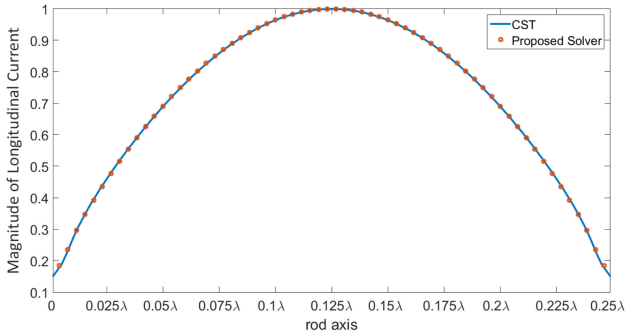


Fig. 7. Normalized longitudinal current coeffieicnts magnitude along the rod of Fig. 6 due to an illumination with a co-polar plane wave with frequency of 193 THz.

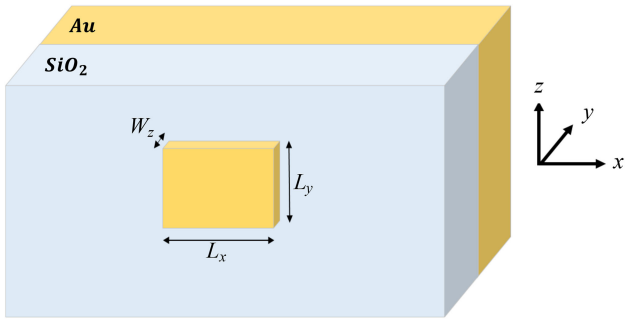


Fig. 8. Gold patch on top of a finite $SiO_2$ substrate backed by a sufficiently thick gold ground layer.

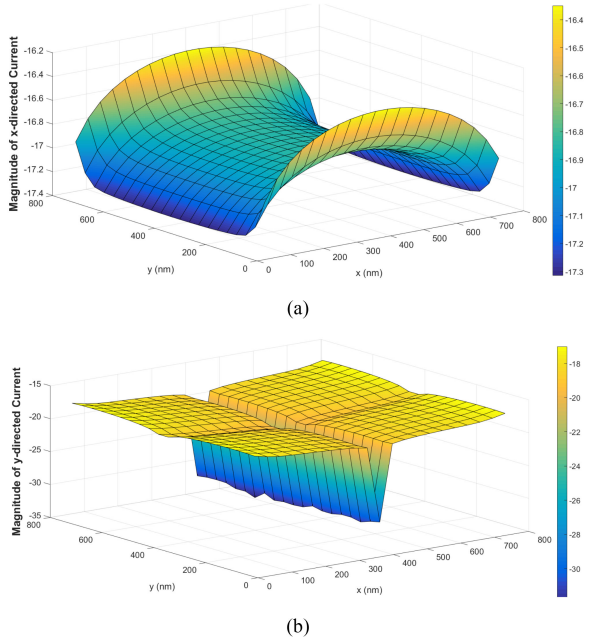


Fig. 9. Logarithm (decade) of the current coeffieicnts magnitude (A.m) over a square patch located above $SiO_2$/Au substrate and excited with a $x$-polarized plane wave with 193 THz frequency: (a) $x$-component and (b) $y$-component.

expected sinusoidal behavior, which is associated with a rod length close to half of a guided wavelength. Current nulls are observed at the open-circuit terminals of the rod. Between the two current nulls at the terminals, the current goes to its maximum value at the center of the rod. The maximum current coefficient magnitude at the center of the rod is $4.34\times10^{-18}$ A.m, which is used for normalization in Fig. 7. It is worth mentioning that exciting a structure with a plane wave allows one to easily obtain the current distribution of the fundamental mode(s) of this structure.

### *B. Plasmonic Nano Square Patch on Top of Finite Substrate and Illuminated by Plane Wave*

The resonator is now in the form of a square gold nano patch on top of the same $SiO_2$/Au substrate, with same thicknesses as in subsection *A*, as shown in Fig. 8. The dimensions of the patch are $L_x = 775$ nm, $L_y = 775$ nm, and $W_z = 77.5$ nm. At $\lambda_0$ of 1550 nm (193 THz), these patch dimensions correspond to 0.5 $\lambda_0$ , 0.5 $\lambda_0$ , and 0.05 $\lambda_0$ , respectively.

Similar to the previous example, this square patch is excited by a 193 THz incident plane wave propagating along $-z$ direction whose electric field is polarized along the $x$-direction with $E_0$ of 1 V/m. The distributions of the $x$- and $y$-components of the induced current over the entire patch are calculated using the proposed solver and plotted in Fig. 9. The patch is meshed such that 21, 21, and 1 segment are taken along $x$-, $y$-, and $z$-directions, respectively. The corresponding memory for this mesh size is 31.7 MB for the proposed solver. As for CST, it requires 248 MB of memory to simulate the same structure.

As expected, the current component parallel to the incident electric field, which is the $x$-component, is dominant. Similar to the rod, half-sinusoidal distribution can be noticed for the dominant current component along the direction of the incident electric field. Along the orthogonal direction, the dominant current component shows significant and rapid increase towards the edges of the patch. Due to the symmetry of the structure, one should expect another perpendicular fundamental mode. Similar patch nano antenna is considered in [50], but fed with a plasmonic transmission line.

### *C. Band-Stop Filter*

The band-stop filter is a two-port structure that prevents specific frequency band from being transferred from one port to the other one. This band is known as the stop-band of the filter. A silver band-stop filter is built above $SiO_2$ substrate with a thickness of 1450 nm and backed by a sufficiently thick silver ground plate, as shown in Fig. 10.

The theory of operation of this device is fairly simple. There two open circuit stubs located at the edges of the vertical rod. At a specific frequency, these two stubs seen as short circuits at the points of intersection between the vertical rod and the feeding horizontal transmission lines. This occurs when the length of these stubs equal quarter of a guided wavelength. Consequently, the current coming from a transmission line is flowing almost totally through the stub, which appears as a short circuit, leaving no current for the other transmission line. The frequency at which this happens is the resonance frequency of the filter, which

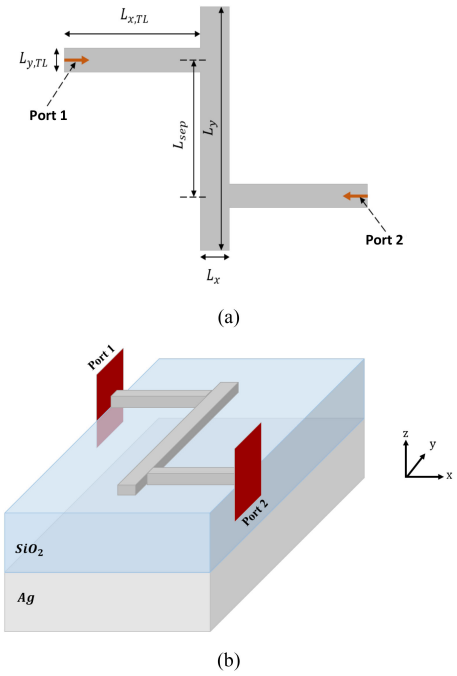


Fig. 10. Silver band-stop filter on top of $SiO_2$ substrate backed by sufficiently thick silver ground layer: (a) Top view and (b) Three-dimensional view.

is located close to the middle of its stop-band. This structure was used in [51] as a microwave band-stop filter. The same structure is reconsidered here for the optical frequency range. The optimum values of the filter's dimensions shown in Fig. 9 to resonate at 193 THz and to match feeding transmission lines with width $L_{y,TL} = 36.15$ nm are: $L_x = 28$ nm, $L_y = 470$ nm, $L_{sep} = 144.61$ nm. The thickness of the structure is $W_z = 26$ nm. The considered length of the feeding transmission lines is $L_{x,TL} = 336$ nm.

The proposed solver is used to analyze the band-stop filter under investigation. The structure is first excited with a roof-top at the edge of the left-hand side transmission line, port 1 in Fig. 10(a). The corresponding current along the structure is calculated. Then, the excitation is applied at port 2, which is located at the far edge of the right-hand-side transmission line and the corresponding current along the structure is also calculated. The currents along the feeding lines, for the two excitations, are expanded as superposition of incident and reflected waves. The weights of these waves are used to calculate the *S*-parameters of the proposed structure [52].

The dimensions of the mesh used for simulating this structure are 12-by-1-by-1 for each horizontal feeding transmission line and 1-by-13-by-1 for the vertical connecting rod. The required memory to simulate this structure by the proposed solver and CST are 139 MB and 958 MB, respectively. The insertion loss, i.e., $S_{21}$, is plotted versus frequency in Fig. 11 as obtained using the proposed solver and CST. $S_{21}$ is defined as the ratio between the transmitted wave to port 2 and the incident wave at port 1, when port 1 is excited and port 2 is terminated with a matched load. The losses along the two transmission lines are de-embedded from the results of the two solvers.

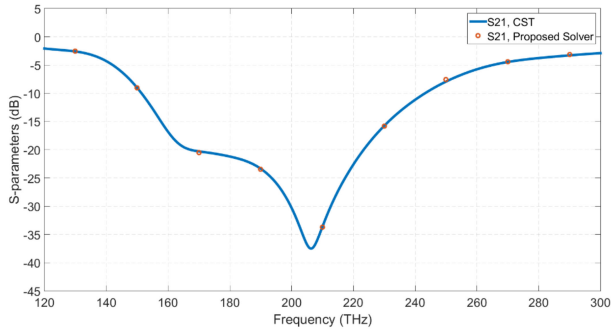


Fig. 11. $S_{21}$ in dB versus frequency in THz for the band-stop filter obtained using both the proposed solver and CST.

Very good agreement can be observed in Fig. 11. $S_{21}$ is lower than $-10$ dB from 150 THz till 240 THz, which is the stop-band of this filter. Normalizing to the central frequency, this bandwidth is equivalent to 46%. Narrower bandwidth down to a few percentages can be achieved if a high-quality resonator is used instead of the simple structure under investigation.

## V. Conclusion

In this study, a volume integral equation formulation for planar plasmonic nano structures in layered media is presented. The thickness of the structures under investigation is accurately taken into account. Layered media of practical importance in plasmonic applications are considered. The Green's functions of these media are fully expressed in the spectral domain. The corresponding spatial domain Green's functions are efficiently obtained by means of Sommerfeld identity and the DCIM. The MoM is used to solve the formulated integral equation. The developed solver based on the presented formulation is applied on different plasmonic structures in layered media. The results show a very good agreement with those obtained using the frequency domain solver of CST Microwave Studio. Since only the localized metal objects are meshed with no need for meshing the surrounding medium, the number of unknowns solved for by the proposed solver is much less than that considered by CST. Consequently, the proposed integral equation solver is about 10 times faster than solvers based on FEM or FDTD. Moreover, the memory needed by the proposed MoM solver is much less than that needed by solvers employing the other two numerical techniques.

## References

[1] K.-S. Lee and M. A. El-Sayed, "Gold and silver nanoparticles in sensing and imaging: Sensitivity of plasmon response to size, shape, and metal composition," *J. Phys. Chem. B*, vol. 110, no. 39, pp. 19220–19225, 2006.

[2] Y.-F. Chou Chao *et al.*, "Perfect dual-band absorber based on plasmonic effect with the cross-hair/nanorod combination," *Nanomaterials*, vol. 10, no. 3, pp. 493, 2020.

[3] C. D'Andea *et al.*, "Optical nanoantennas for multiband surface-enhanced infrared and Raman spectroscopy," *ACS Nano*, vol. 7, no. 4, pp. 3522–3531, 2013.

[4] X. Wang, S. C. Huang, S. Hu, S. Yan, and B. Ren, "Fundamental understanding and applications of plasmon-enhanced Raman spectroscopy," *Nature Rev. Phys.*, vol. 2, no. 5, pp. 253–271, 2020.

[5] L. J. Sherry, R. Jin, C. A. Mirkin, G. C. Schatz, and R. P. V. Duyne, "Localized surface plasmon resonance spectroscopy of single silver triangular nanoprisms," *Nano Lett.*, vol. 6, no. 9, pp. 2060–2065, 2006.

[6] P. Bharadwaj, B. Deutsch, and L. Novotny, "Optical antennas," *Adv. Opt. Photon.*, vol. 1, no. 3, pp. 438–483, 2009.

[7] Y. F. Chou Chau *et al.*, "Tunable optical performances on a periodic array of plasmonic bowtie nanoantennas with hollow cavities," *Nanoscale Res. Lett.*, vol. 11, no. 1, 2016, Art. no. 7.

[8] M. Donelli, "Design of broadband metal nanosphere antenna arrays with a hybrid evolutionary algorithm," *Opt. Lett.*, vol. 38, no. 4, pp. 401–403, 2013.

[9] E. A. Soliman, "Wideband nanocrescent plasmonic antenna with engineered spectral response," *Microw. Opt. Tech. Lett.*, vol. 55, no. 3, pp. 624–629, Mar. 2013.

[10] M. H. El-Sherif, M. H. Bakr, and E. A. Soliman, "E-shaped wideband plasmonic nantennas with linear and dual-linear polarizations," *Photon. Res.*, vol. 3, no. 4, pp. 140–145, Aug. 2015.

[11] E. A. Soliman, M. O. Sallam, and G. A. E. Vandenbosch, "Plasmonic grid array of gold nano-rods for point-to-point optical communications," *J. Lightw. Technol.*, vol. 32, no. 24, pp. 4296–4302, Dec. 2014.

[12] M. C.-Lopez, N. de Sousa, A. G.-Martin, Y. F. Gardes, and R. Sapienza, "Scattering of a plasmonic nanoantenna embedded in a silicon waveguide," *Opt. Exp.*, vol. 23, no. 22, pp. 28108–28118, 2015.

[13] L. Yin *et al.*, "Subwavelength focusing and guiding of surface plasmons," *Nano. Lett.*, vol. 5, no. 7, pp. 1399–1402, 2005.

[14] Z. Liu, J. M. Steele, W. Srituravanich, Y. Pikus, C. Sun, and X. Zhang, "Focusing surface plasmons with a plasmonic lens," *Nano Lett*, vol. 5, no. 9, pp. 1726–1729, 2005.

[15] Y. F. Chou Chau *et al.*, "Significantly enhanced coupling effect and gap plasmon resonance in a MIM-cavity based sensing structure," *Sci. Rep.*, vol. 11, no. 1, 2021, Art. no. 18515.

[16] P. Berini, "Plasmon-polariton modes guided by a metal film of finite width bounded by different dielectrics," *Opt. Exp.*, vol. 7, no. 10, pp. 329–335, 2000.

[17] P. Deng, W. Hong, and X. H.-Xing, "Metallic nanowires for subwavelength waveguiding and nanophotonic devices," *Chin. Phys. B*, vol. 22, no. 9, 2013, Art. no. 097305.

[18] L.-Z. Hsieh *et al.*, "Metal nano-particles sizing by thermal annealing for the enhancement of surface plasmon effects in thin-film solar cells application," *Opt. Commun.*, vol. 370, pp. 85–90, 2016.

[19] R. A. Pala, J. White, E. Barnard, J. Liu, and M. L. Brongersma, "Design of plasmonic thin-film solar cells with broadband absorption enhancements," *Adv. Mater.*, vol. 21, no. 34, pp. 3504–3509, 2009.

[20] H. A. Atwater and A. Polman, "Plasmonics for improved photovoltaic devices," *Nature Mater.*, vol. 9, pp. 205–213, 2010.

[21] S. A. Maier, *Plasmonics: Fundamentals and Applications*. Berlin, Germany: Springer, 2007.

[22] J. M. Jin, *Theory and Computation of Electromagnetic Fields*. Hoboken, New Jersey, USA: Wiley, 2015.

[23] P. Monk, *Finite Element Methods for Maxwell's Equations*. Oxford, U.K.: Oxford Univ. Press, 2003.

[24] C.-T. Chou Chao *et al.*, "Highly sensitive and tunable plasmonic sensor based on a nanoring resonator with silver nanorods," *Nanomaterials*, vol. 10, no. 7, 2020, Art. no. 1399.

[25] Y.-F. Chau and D. P. Tsai, "Three-dimensional analysis of silver nanoparticles doping effects on super resolution near-field structure," *Opt. Commun.*, vol. 269, no. 2, pp. 389–394, 2007.

[26] D. F. P. Pile, D. K. Gramotnev, M. Haraguchi, T. Okamoto, and M. Fukui, "Numerical analysis of coupled wedge plasmons in a structure of two metal wedges separated by a gap," *J. Appl. Phys.*, vol. 100, no. 1, 2006, Art. no. 013101.

[27] R. F. Harrington, *Field Computation by Moment Methods*. New York, NY, USA: Macmillan, 1968.

[28] E. A. Soliman, "Semi-analytical calculation for sensitivities of the method of moments impedance and excitation matrices," *Int. J. RF Microw. Comput. Aided Eng.*, vol. 17, no. 6, pp. 533–541, 2007.

[29] E. A. Soliman, M. H. Bakr, and N. K. Nikolova, "Neural networks-method of moments (NN-MoM) for the efficient filling of the coupling matrix," *IEEE Trans. Antennas Propag.*, vol. 52, no. 6, pp. 1521–1529, Jun. 2004.

[30] A. A. Sakr, E. A. Soliman, and A. K. Abdelmageed, "A surface integral equation formulation for electromagnetic scattering from a conducting cylinder coated with multilayers of homogeneous materials," *J. Appl. Phys.*, vol. 116, no. 5, 2014, Art. no. 054902.

[31] A. M. Kern and O. J. F. Martin, "Surface integral formulation for 3D simulations of plasmonic and high permittivity nanostructures," *J. Opt. Soc. Amer.*, vol. 26, no. 4, pp. 732–740, Apr. 2009.

[32] D. M. Solis, J. M. Taboada, and F. O. Basteiro, "Surface integral equation-method of moments with multiregion basis functions applied to plasmonics," *IEEE Trans. Antennas Propag.*, vol. 63, no. 5, pp. 2141–2152, May 2015.

[33] I. Sekulic, D. C. Tzarouchis, P. Ylä-Oijala, E. Ubeda, and J. M. Rius, "Enhanced discretization of surface integral equations for resonant scattering analysis of sharp-edged plasmonic nanoparticles," *Phys. Rev. B*, vol. 99, Apr. 2019, Art. no. 165417.

[34] M. G. Araújo, J. M. Taboada, D. M. Soliś, J. Rivero, L. Landesa, and F. Obelleiro, "Comparison of surface integral equation formulations for electromagnetic analysis of plasmonic nanoscatterers," *Opt. Exp.*, vol. 20, pp. 9161–9171, Apr. 2012.

[35] H. Gómez-Sousa, Ó. Rubiños-López, and J.Á. Martiñez-Lorenzo, "Comparison of iterative solvers for electromagnetic analysis of plasmonic nanostructures using multiple surface integral equation formulations," *J. Electromagn. Waves Appl.*, vol. 30, pp. 456–472, Feb. 2016.

[36] M. O. Sallam, G. A. E. Vandenbosch, G. Gielen, and E. A. Soliman, "Integral equations formulation of plasmonic transmission lines," *Opt. Exp.*, vol. 22, no. 19, pp. 22388–22402, Sep. 2014.

[37] M. O. Sallam, G. A. E. Vandenbosch, G. Gielen, and E. A. Soliman, "Generalized mode solver for plasmonic tranmission lines embedded in layered media based on the method of moments," *Comput. Phys. Commun.*, vol. 233, pp. 1–15, Dec. 2018.

[38] W.-B. Ewe, H.-S. Chu, and E.-P. Li, "Volume integral equation analysis of surface plasmon resonance of nanoparticles," *Opt. Exp.*, vol. 15, pp. 18200–18208, Dec. 2007.

[39] R. Remis and E. Charbon, "An electric field volume integral equation approach to simulate surface plasmon polaritons," *Adv. Electromagn.*, vol. 2, pp. 15–24, 2013.

[40] A. M. Lerer, I. V. Donets, G. A. Kalinchenko, and P. V. Makhno, "Volume integral method for investigation of plasmonic nanowaveguide structures and photonic crystals," *Photon. Res.*, vol. 2, pp. 31–37, Feb. 2014.

[41] Z. He, J. Hong Gu, W. E. I. Sha, and R. Shan Chen, "Efficient volumetric method of moments for modeling plasmonic thin-film solar cells with periodic structures," *Opt. Exp.*, vol. 26, pp. 25037–25046, Sep. 2018.

[42] CST Microwave Studio. 2022. [Online]. Available: www.cst.com

[43] Y. L. Chow, J. J. Yang, D. G. Fang, and G. E. Howard, "A closed-form spatial Green's function for the thick microstrip substrate," *IEEE Trans. Microw. Theory Techn.*, vol. 39, no. 3, pp. 588–592, Mar. 1991.

[44] Y. Hua and T. K. Sarkar, "Generalized pencil-of-function method for extracting poles of an EM system from its transient response," *IEEE Trans. Antennas Propag.*, vol. 37, no. 2, pp. 229–234, Feb. 1989.

[45] R. W. Hamming, *Numerical Methods For Scientists and Engineers*. New York, NY, USA: Dover, 1973.

[46] J. L. Volakis and K. Sertel, *Integral Equation Methods for Electromagnetics*. Raleigh, NC, USA: SciTech Publishing, 2012.

[47] E. A. Soliman, M. A. El-Gamal, and A. K. Abdelmageed, "Neural network model for the efficient calculation of Green's functions in layered media," *Int. J. RF Microw. Comput. Aided Eng.*, vol. 13, no. 2, pp. 128–135, Mar. 2003.

[48] P. B. Johnson and R. W. Christy, "Optical constants of the noble metals," *Phys. Rev. B*, vol. 6, no. 12, pp. 4370–4379, Dec. 1972.

[49] E. A. Soliman, A. K. Abdelmageed, and M. A. El-Gamal, "Neural computation of the MoM matrix elements for planar configurations," *Int. J. Electron. Commun.*, vol. 56, no. 3, pp. 155–262, Mar. 2002.

[50] E. M. Mahdy, A. K. Abdelmageed, and E. A. Soliman, "Integral equation formulation for planar plasmonic nano structures in layered media," in *Proc. Eur. Conf. Antennas Propag.*, Copenhagen, Denmark, Mar. 2020, pp. 1–5.

[51] E. A. Soliman, M. H. Bakr, and N. K. Nikolova, "Accelerated gradient-based optimization of planar circuits," *IEEE Trans. Antennas Propag.*, vol. 53, no. 2, pp. 880–883, Feb. 2005.

[52] E. A. Soliman, G. A. E. Vandenbosch, E. Beyne, and R. P. Mertens, "Multimodal characterization of planar microwave structures," *IEEE Trans. Microw. Theory Techn.*, vol. 52, no. 1, pp. 175–182, Jan. 2004.